International Journal of Remote Sensing

Comparison between automated and manual mapping of typhoon-triggered landslides from SPOT-5 imagery

A. M. Borghuis [a]; K. Chang [b]; H. Y. Lee [c]
a Utrecht University, Department of Physical Geography, The Netherlands
b Department of Geography, National Taiwan University, Taipei, Taiwan 106
c Department of Civil Engineering, National Taiwan University, Taipei, Taiwan 106

PLEASE SCROLL DOWN FOR ARTICLE

Taylor & Francis
Taylor & Francis Group

Comparison between automated and manual mapping of typhoon-triggered landslides from SPOT-5 imagery

A. M. BORGHUIS†, K. CHANG*‡ and H. Y. LEE§

†Utrecht University, Department of Physical Geography, The Netherlands
‡Department of Geography, National Taiwan University, Taipei, Taiwan 106
§Department of Civil Engineering, National Taiwan University, Taipei, Taiwan 106

Two large tropical cyclones struck Taiwan in the summer of 2004 and landslides triggered by these events caused not only casualties and housing damage but also produced large volumes of sediment that entered rivers and reservoirs. For reservoir and watershed management it is important to quickly identify the location and areal extent of new landslides for coordinating mitigation efforts. In this study, two automated methods, supervised and unsupervised classification of 10 m multi-spectral SPOT-5 imagery, were tested for their ability to identify and map landslide areas before and after the two storm events. A slope map was applied to mask roads, riverbeds and agricultural fields erroneously commissioned as landslides. The automated classification results were compared with manually delineated landslides using SPOT-5 supermode satellite imagery with a resolution of 2.5 m. Statistical testing and spatial analysis of the mapping results were performed. Finally, the results from all three methods were validated by using 0.35 m orthophotographs. This paper reports the results and discusses the salient differences between the automated and manual methods.

1. Introduction

Taiwan is an island, about 380 km long and 140 km wide, separated by the Strait of Formosa from southeastern China. The island is prone to an average of four to five tropical cyclones, also called typhoons, each year. These intense storms bring torrential rains that trigger landslides in the mountain belt that runs north–south, occupying almost two thirds of the island (figure 1). In the second half of the 20th century, a number of hydro-electric dams were constructed in the forested mountain areas across the island. Over the years, landslides have scoured hill slopes and acted as major sources of both coarse and fine sediments in channels and rivers. These sediments have been transported and deposited in dams and reservoirs, reducing their storage capacity for drinking water and/or electricity production. A local assessment indicated that between 8.8% and 9.7% of all sediment is trapped by reservoirs annually (Hwang 1994). Studies have further shown that landslides contribute to the majority of sediments that enter the reservoir, especially in well-forested watersheds where soil erosion rates are relatively low (e.g. Borghuis and Chiu 2005). This is why rapid and accurate identification of new landslides is of great importance to support watershed management. A quick response can enable

---

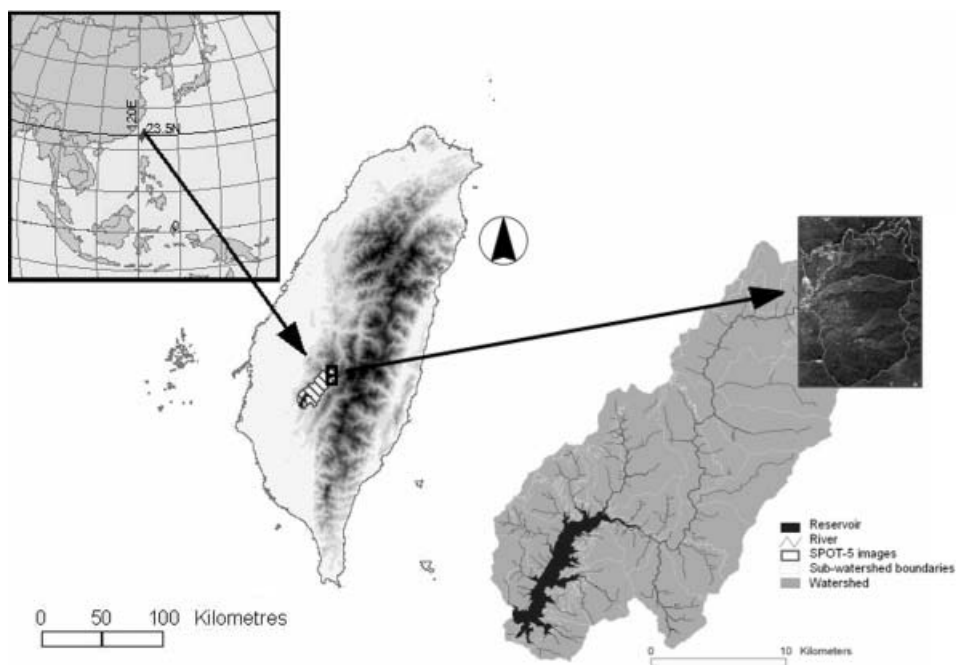*Corresponding author. Email: ktchang@ntu.edu.tw

Figure 1.   Location of the study area in Taiwan.

the timely removal of landslide deposits or application of protective measures for preventing further downslope rock and soil transport.

Aerial photographs have long been used to interpret and delineate landslides. But mapping landslides using aerial photographs is a tedious and time-consuming process. In recent years, researchers have turned to satellite images as a data source for mapping landslides using methods that range from visual interpretations to semi-automatic approaches. Following this recent trend, the main objective of this study is to test whether recent satellite imagery can be a source for accurate and cost-efficient identification of landslides. For this purpose 10 m SPOT-5 multi-spectral imagery and 2.5 m supermode imagery were obtained. The study involved four main tasks. First, we tested the supervised and unsupervised classification methods to identify landslides on the multi-spectral imagery. Second, we delineated landslides manually from the supermode satellite images. Third, statistical tests and spatial analysis were performed to evaluate and to better understand the differences found in the landslide mapping results. Finally, by using a set of 0.35 m resolution digital orthophotographs, two-thirds of all landslides mapped by the automated and manual methods were validated. Findings from this study should be of interest to landslide researchers as well as watershed management agencies.

2.   Landslide mapping

2.1   *Landslides*

The term 'landslide' describes a downslope movement of a mass of soil and rock material (Cruden 1991). Various landslide classifications by morphology, material, mechanism of initiation and other criteria are available. In general landslide types include rock falls, rock slides, earth flows, earth slides and debris flows. Landslides

are usually triggered by earthquakes, storms or human activities such as road construction or a combination of these factors (Aleotti and Chowdhury 1999). Morphologies typical of slope movements such as scarps, deposit zones, disturbed vegetation and disturbed channels or roads provide visual cues that are important for manually interpreting landslides on an aerial photograph or satellite image (Dikau 1999).

2.2 *Manual delineation from aerial photographs*

Traditionally, aerial photographs are used to identify and delineate landslides and to produce landslide inventory maps. With high details in aerial photographs, zones of previous sliding activities can easily be identified by their characteristic scarps and debris flow deposits. But use of aerial photographs for landslide mapping has several disadvantages. First, aerial photographs cover relatively small areas and many photographs are needed to cover a large watershed. Second, manual delineation of landslides is a tedious and expensive job. For example, Liu and Woing (1999) cited one study, in which 100 work-days were required to identify over 4000 landslides on stereo aerial photographs, manually delineate landslide boundaries and add landslides to a GIS (geographical information system) database. Third, clouds, especially in sub-tropical mountain areas, inevitably will obscure part of the imagery. Finally, the recurrence interval of aerial photographs is often irregular, especially for mountainous forest areas with little commercial value, and, as the recurrence interval prolongs vegetation re-growth and man-made protective covers can make it difficult or impossible to identify new landslides (Korup 2004).

2.3 *Previous satellite image based studies*

Compared to aerial photographs, satellite images have two distinct advantages. They usually have recurrence intervals of days. And, based on our experience, obtaining cloud-free satellite imagery close to the storm event date is relatively easy and can be done online, allowing a preview of images before acquiring them. It is therefore no surprise that satellite images, especially those of high-resolution, have replaced aerial photographs for mapping landslides in recent years. For example, the Soil and Water Conservation Bureau of Taiwan has used SPOT-5 products to compile landslide inventory maps for the past few years. However, few satellite-based methods for automated landslide detection have been tested so far.

Petley *et al.* (2002) used Landsat 7 ETM + imagery to map landslides in upland areas of Nepal and Bhutan. They found that the image classification missed more than 75% of landslides detected by the ground mapping method. Major problems, according to them, were the spatial resolution of Landsat 7 ETM +, the spectral resolution, the shadowed slopes and the rugged terrain. Haeberlin *et al.* (2004) reported that SPOT-5 products can be helpful for determining large, kilometre-sized slope instabilities in Nicaragua but semi-automatic approaches based on image radiometry does not seem appropriate for mapping landslides.

Nichols and Wong (2004) tested and validated a multi-temporal approach for landslide change detection using SPOT imagery. They reported detection rates up to 70%. Because their study area was mostly uncultivated, the only changes in the images were new landslides. They also found that 80% of landslides had trails no wider than 10 m. The same paper presented a number of image fusion techniques

involving pan-sharpened IKONOS imagery, which supposedly can obtain the same or better image results for detailed mapping and interpretation as traditional aerial photographs. Dadson *et al.* (2004) used 20 m SPOT-4 satellite imagery and identified 20 000 soil and bedrock landslides within a total area of 150 km^2 in central Taiwan. They claimed that the 20 m resolution allowed landslides larger than 3600 m^2 (3×3 pixels) to be mapped accurately. But omission of smaller landslides might have caused significant underestimation of disturbed areas.

It becomes clear from previous studies that multi-spectral satellite images are potentially useful for mapping landslides at the regional scale. However, the spatial resolution has been a major problem. Recent medium- and high-resolution multi-spectral scanners on platforms such as IKONOS, Quickbird and SPOT-5 appear to have filled this gap (Vohora and Donoghue 2004, Chadwick *et al.* 2005, Rosin and Hervás 2005). In addition, the use of filters, masks and colour composites can also assist in classifying landslides on satellite images (Petley *et al.* 2002, Haeberlin *et al.* 2004, Ramli and Petley 2006). But more empirical evidence is needed, and it is important to continue testing automated methods on new satellite image sources.

3. Data

3.1 *Study area*

The study area, measuring 115 km^2 in size, is located in southern Taiwan in the upstream part of the Tsengwen reservoir watershed (figure 1). The area consists of two sub-watersheds with a common outlet after the confluence of the major draining streams at the so-called Da-Bang dam, located just outside the study area on the west side. More than 90% of the study area is covered by tropical forest vegetation, with the remaining area occupied by small settlements and agricultural fields. One major stream flows in the northeast to southwest direction, while two tributaries join the main stream in the west, draining the east and southeastern parts of the watershed. The topography is generally rugged, with elevations ranging from 765 m to 2611 m and slope angles ranging from 0° to over 56° (figure 2). The 1 : 250 000 scale geological map shows the area is dominated by Late-Miocene sandstones, while the central part of the study area features Middle-Miocene sandstones and coal layer seams. Overlaying soils have a stony character. Field sampling shows that soils are in most cases at least 0.40 m in depth. The top often consists of up to 0.05 m thick organic material and a generally well developed A-horizon under bamboo and dense mixed tropical forest stands.

3.2 *Typhoons*

Typhoon Mindulle passed by Taiwan from the south affecting the island for four days (28 June–3 July). Typhoon Mindulle brought about 1182 mm of rain to the study area, with a maximum intensity of 905 mm recorded over a 24-hour period (CWB 2004a). Typhoon Aere (23–26 August) crossed the northern tip of the island in an east–west direction, causing severe damage in terms of loss of life, property and landslides. During typhoon Aere, 784 mm fell in the study area, with a maximum intensity of 486 mm over 24 hours (CWB 2004b). Two other typhoons (Kompasu and Rananim) also passed by Taiwan in the 2004 typhoon season between Mindulle and Aere but did not bring any significant rain to the study area (2.5 mm and 32 mm, respectively).
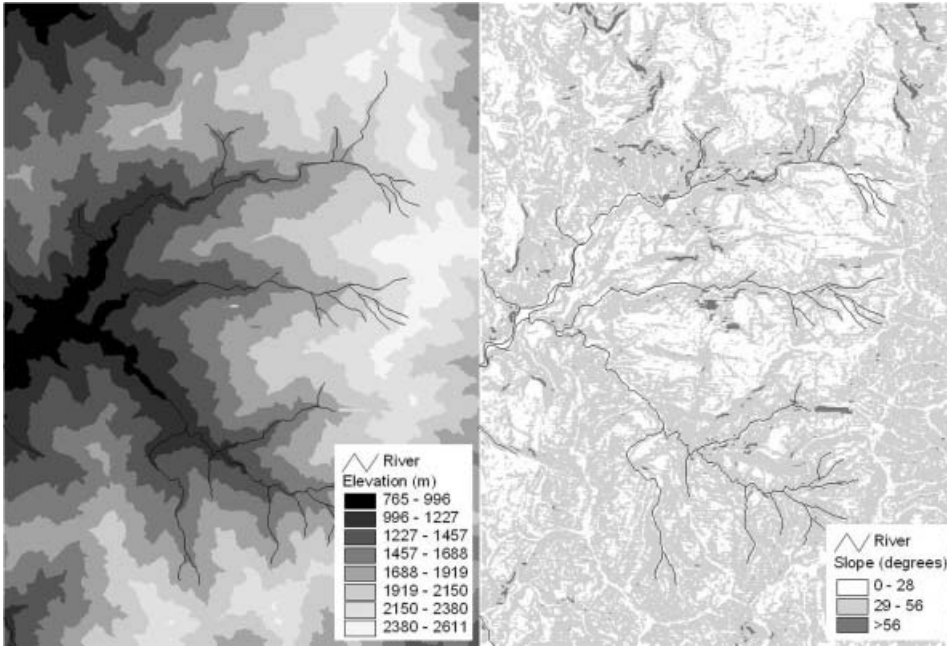
Figure 2.   Elevation and slope map of the study area.

3.3   *Satellite images*

SPOT-5 images were obtained to assess the extent of landslides in the study area caused by typhoons Mindulle and Aere, respectively, in the summer of 2004. Three images were selected, one before and one after each typhoon event, so that the impact of each typhoon on the study area could be assessed. A 99% cloud-free image on 12 April was selected to investigate the initial conditions before typhoons Mindulle and Aere struck. The 10 July image was taken just seven days after typhoon Mindulle left Taiwan, and a third image on 12 October showed the conditions after typhoon Aere passed through northern Taiwan.

The SPOT-5 imagery consisted of two different modes for the same scene. The so-called supermode produced detailed colour images using two parallel scanners, each with a 5 m resolution. After processing, an interpolated image with a resolution of 2.5 m was derived. In addition, 10 m multi-spectral images of the same scene were obtained for the automated classifications. The multi-spectral imagery consisted of the green, red, near-infrared and short-wave infrared wavelength bands. The short-wave infrared band had an original resolution of 20 m and was resampled to 10 m.

4.   Methods

This study tested two automated techniques for landslide identification, supervised and unsupervised classification, and manual delineation. Free and open-source GRASS GIS was used for the automated classifications, while ESRI's ArcGIS was employed for overlay, area calculation, data conversion and geospatial data management.

Before any classification was made, the 10 m multi-spectral imagery was used to calculate the Normalized Difference Vegetation Index (NDVI) for each scene (Lillesand *et al.* 2004). We used the NDVI to quickly find sparsely vegetated areas, possibly caused by landslides (Liu *et al.* 2002). Dark grey or black areas with negative grid cell values would indicate areas with sparse or no vegetation, such as landslides, rivers, roads, towns and barren farmland. Contrasting light grey and white areas would indicate healthy forest and vegetation. NDVI values ranged from −0.44 to 0.54 on 12 April, from −0.34 to 0.73 on 10 July and from −0.4 to 0.61 on 12 October. As one might expect, vegetation in early summer appeared greener than in early spring, while the autumn image showed a slight decrease in overall vegetation indices from early summer. The dry river floodplains, as well as roads and towns, were clearly visible in all NDVI results. The NDVI results were used to support the manual delineation by giving some directions as to where to search for landslides in the 2.5 m supermode imagery.

4.1 *Unsupervised classification*

Using the unsupervised classification method, our first task was to find a number of classes that could separate landslides from other land use types. All unsupervised classifications were performed using a combination of all available wavelength bands (bands 1, 2, 3 and 4) and by employing a maximum-likelihood classifier (MLC) (Neteler and Mitasova 2004). By classifying the image into eight classes we found that landslides could not be distinguished from dry riverbeds, roads and bare farm fields, which apparently had spectral properties that were similar to landslide areas. When we increased the number of classes to 32, the result was better than for eight classes. However, we found that still no 'pure' landslide classes were created.

A solution to this problem was to filter out those areas that were not landslides. Because many wrongly classified features were in reality farmland, roads or houses, a method had to be found that could mask these features while not obscuring landslide areas. It was decided to try an overlay of the unsupervised results with a slope map of the study area. The idea was that most built-up areas, roads, farmland and also riverbeds have relatively low slope angles, while landslides are mostly associated with steep slopes (e.g. Chang and Slaymaker 2002). Further investigation revealed a law ordered by the Soil and Water Conservation Bureau, forbidding all construction or new farmland on slopes greater than 28° (SWCB 2003).

We calculated slopes from a digital elevation model (DEM) with a 40 m resolution (standard DEM in Taiwan) and tested the 28° limit. At 28°, landslides were still correctly classified, while barren farmland or roads, houses and dry riverbeds were successfully excluded. A 25° slope mask would include too many road or farmland cells while a 30° slope mask would exclude areas identified in the field as parts of landslides. The result of experimentation convinced us to use a mask of all cells with a slope of less than 28° to filter out non-landslide areas in an unsupervised classification.

In addition to the slope filter, we also used a 'noise filter' to remove isolated small groups of pixels or individual pixels that were classified as landslides but were too small to possibly be landslides. In effect, this filter enforced a minimum (landslide) mapping unit. We used a maximum of three adjacent pixels for the noise filter, meaning that all areas less than 300 m^2 and a length or width less than 30 m were excluded from the classification result.

4.2 *Supervised classification*

In this study we decided to obtain training areas for four classes: rock (dry riverbed), existing landslide, forest and urban area. For forest, a number of training areas were used since forests appeared differently for various parts of the study area due to shadows and different vegetation types. For landslides, the training areas consisted of a large landslide and a small landslide that were visited in the field. For rock, bare rocks in the river as well as rocks that could be seen in the image and confirmed in the field were used. The largest town in the study area was chosen to be the training area for the urban land use class. A MLC then used the spectral signatures of the training areas to assign each cell in the image the class with the highest probability. Similar to the unsupervised classification, the supervised classification also used a 28° slope mask and a noise filter of three pixels.

4.3 *Manual classification*

We used the SPOT-5 2.5 m supermode imagery for the manual delineation. The 2.5 m resolution enabled identification of features in the image such as single houses, farm land, roads and landslides. First, an initial rough classification of areas and features in each image was performed in order to identify farms, buildings, rock cliffs and clouds, besides landslides. The aforementioned NDVI layer assisted in the identification process. Rock cliffs could easily be distinguished from landslides since they lacked the typical scar left by a mass movement. It was, however, more difficult to identify small landslides, especially those along roads and streams. Subsequently, all features that were identified as landslides were digitized on screen in a GIS (Chang 2006).

4.4 *Analysis of landslide area*

We used the *t*-test to determine whether or not there were significant differences in mean landslide areas generated by the three methods for the three image dates. In addition, the area concordance measured how well landslide areas mapped by the three methods overlapped. Expressed as a percentage, the area concordance is calculated by: [(overlapped landslide area)/(total landslide area mapped by the manual method)]*100, where the overlapped landslide area represents the intersection of landslides from the manual method and the automated method(s). The manually delineated landslide polygons were converted to 10 m raster cells for the analysis.

The area concordance is based on landslide areas only. It is different from a confusion matrix for image analysis, which in this case would be based on landslide and non-landslide areas. Landslide areas as mapped by the three methods range from only 0.34% to 1.80% of the total study area. Any quantitative measures derived from a confusion matrix would therefore be strongly biased towards non-landslide areas. This is why the area concordance was adopted for this study as a simple, appropriate measure of the overlap of landslide areas.

4.5 *Validation by orthophotographs*

We used digital colour orthophotographs to validate landslides delineated by the manual and automated methods from SPOT-5 products and to explain their differences. These orthophotographs were compiled from stereo pairs of 1:5000

aerial photographs by the Aerial Survey Office of Taiwan's Forestry Bureau. They have a pixel size of 0.35 m and an estimated horizontal accuracy of 0.5 m.

The digital orthophotographs covered more than over 67% of all landslides that were identified by any of the three methods. This large subset allowed us to find landslides that were missed by the automated and manual methods (errors of omission) and areas that were wrongly classified as landslides (errors of commission). The checking was done by eye, and performed by two trained image interpreters.

5. Results

5.1 *Landslide areas*

Figure 3 shows manually delineated landslides and the typical non-vegetated features present in the study area such as river floodplains, towns, bedrock outcrops or cliffs, farm fields and roads.

Tables 1–3 show the total landslide area and the descriptive statistics of individual landslides delineated by the two automated classification techniques and the manual delineation. Several trends are apparent in the tabulated monthly data. First, the total landslide area delineated manually is smaller than those by the automated classifications. Second, tables 1–3 show that the mean landslide area for the manual method is larger than those for the automated methods. The results of *t*-tests are presented in table 4. The difference in the landslide area means between the manual and automated methods are significant, while the differences between the automated methods are not. Third, the manual method records a much smaller number of landslides than the two automated classifications. Fourth, the maximum area of individual landslides is larger for the manual method and the unsupervised classification than the supervised classification.

5.2 *Area concordance*

Table 5 lists measures of the area concordance of landslides as mapped by the automated methods and the manual method. The table shows three types of overlay: landslide areas from all three methods, between the supervised classification and the manual delineation and between the unsupervised classification and the manual delineation. As expected, the overlay of all three methods has the lowest area concordance values. The overlay between the unsupervised classification method and the manual method has the highest area concordance values, ranging from 53% to 63%.

5.3 *Validation*

Orthophotographs were used for validating over 67% of all landslides delineated by the manual method and those identified by the automated methods. The validation of manual delineation results revealed no errors of commission for large landslides but found many errors of omission for small landslides. In contrast, the validation of the automated methods showed more errors of commission but only few errors of omission. Erroneously commissioned areas by the automated methods were found to be primarily stretches of roads, bare soil on farm fields and riverbeds.

Figure 4 illustrates differences between the unsupervised method and the manual method. Figure 4(*a*) shows a series of small landslides along a stream channel. These

Figure 3. Delineated landslides (white outline) in 2.5 m SPOT-5 imagery.

small landslides were correctly identified by the automated method, as shown by the black areas in figure 4(*b*), but were omitted by the manual method. Figure 4(*c*) displays errors of commission made by the automated method; the small black areas identified as landslides were in fact stretches of roads. Figure 4(*d*) shows general areas

Table 1. Supervised classification (MLC) using all bands and slope and noise filters.

Date	12 April 2004	10 July 2004	12 October 2004
Statistics	Total/Mean/Min/Max/SD	Total/Mean/Min/Max/SD	Total/Mean/Min/Max/SD
Area (ha)	61.8/0.11/0.06/3.64/0.29	197/0.14/0.06/7.67/0.39	103/0.18/0.06/6.98/0.48
No. of landslides	540	1428	566

Table 2. Unsupervised classification (MLC) using all bands and slope and noise filters

Date	12 April 2004	10 July 2004	12 October 2004
Statistics	Total/Mean/Min/Max/SD	Total/Mean/Min/Max/SD	Total/Mean/Min/Max/SD
Area (ha)	74.7/0.12/0.06/14.37/0.61	127/0.12/0.06/24.61/0.82	154/0.20/0.06/19.53/0.91
No. of landslides	649	1104	758

Table 3. Manual delineation of landslides using SPOT-5 2.5 m supermode imagery.

Date	12 April 2004	10 July 2004	12 October 2004
Statistics	Total/Mean/Min/Max/SD	Total/Mean/Min/Max/SD	Total/Mean/Min/Max/SD
Area (ha)	39.3/1.57/0.13/18.70/3.63	94.6/1.31/0.02/22.98/3.07	99.4/1.29/0.02/24.89/3.20
No. of landslides	25	72	77

Table 4. Results of *t*-tests for differences of landslide area means.

Methods	12 April 2004	10 July 2004	12 October 2004
Supervised/Unsupervised	$p=0.28$ (df=1182)	$p=0.30$ (df=1174)	$p=0.34$ (df=1310)
Unsupervised/Manual	$p=0.03$ (df=671)	$p=0.00$ (df=2503)	$p=0.04$ (df=757)
Supervised/Manual	$p=0.03$ (df=557)	$p=0.00$ (df=1471)	$p=0.03$ (df=577)

Table 5. Measures of landslide area concordance.

Overlay	12 April 2004	10 July 2004	12 October 2004
All three methods	14.3	20.2	37.6
Supervised/Manual	15.7	37.6	39.4
Unsupervised/Manual	58.6	53.3	63.1

of concordance between the automated method (black areas) and the manual method (white outlines). The landslide at the bottom of figure 4(*d*) also exhibits an important difference between the methods. The manual method produced a single, enclosed landslide whereas the automated method resulted in a fragmented landslide.

6. Discussion

An important finding of the study is that both the supervised and unsupervised classification produced many more small landslides than the manual delineation. This was further confirmed by the *t*-tests for all landslide areas. The differences in landslide areas and numbers can be explained as follows. First, in the manual delineation we connected all areas that appeared to belong to one single landslide, leading to fewer and larger landslides. In contrast, the raster-based automated classification methods identified landslides on a cell-by-cell basis. Large landslides were therefore split into smaller fractions when, for example, patches of vegetation were present on the landslide surface. Second, despite the use of a slope filter, parts of farmland, stretches of roads or parts of riverbeds were still erroneously commissioned as landslides, leading to a high number of small landslides (figure 5). Because of the incorrect classification of roads and riverbeds, the automated
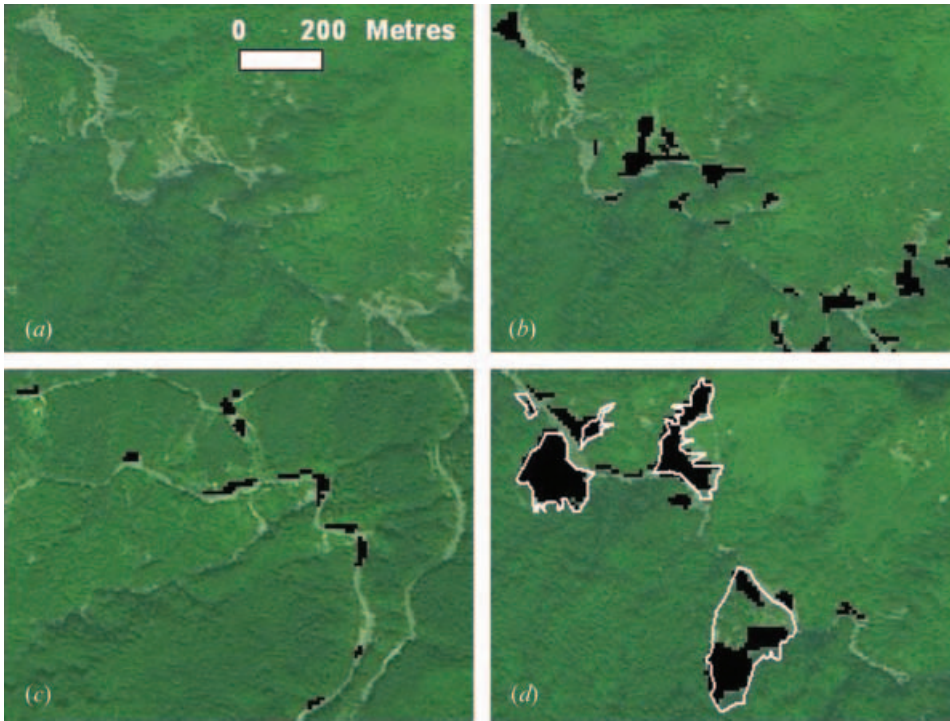
Figure 4.   (*a*) Small landslides along a stream. (*b*) The landslides in (*a*) correctly identified by the automated method. (*c*) Errors of commission by the automated method caused by roads. (*d*) Area concordance between the manual and automated methods.

classification methods likely overestimated the number and areal extent of landslides. Third, we found that the manual delineation of supermode 2.5 m imagery proved not suitable for the identification of small landslides. As a rule, landslides smaller than $400 \, m^2$ (8×8 or 64 pixels) could not be distinguished by eye in the supermode colour images. However, towns, farms and clouds could be easily identified.

The area concordance statistics show large differences between the supervised and unsupervised classifications compared to the manual delineation. The supervised classification result was especially poor (an area concordance of 16%) for the April scene because of the absence of fresh landslides. We used two existing landslides, which we visited in the field, as training areas. The first was a partly re-vegetated landslide appearing very similar to areas where vegetation was still sparse in April. The second was a large and scarcely vegetated landslide with exposed rock materials that appeared to be spectrally similar to the sediment in the dry river floodplain. The result was that many areas were wrongly commissioned as landslides in the April scene.

The difference in the area concordance results between the two methods can be further explained by examining maximum landslide areas in tables 1–3. Landslides generated by the supervised classification are all relatively small and fragmented, with maximum areas ranging from 3.48 ha to 7.67 ha, whereas landslides generated by the unsupervised classification are much larger, with maximum areas ranging from 14.37 ha to 24.61 ha, a range similar to that obtained by the manual method,
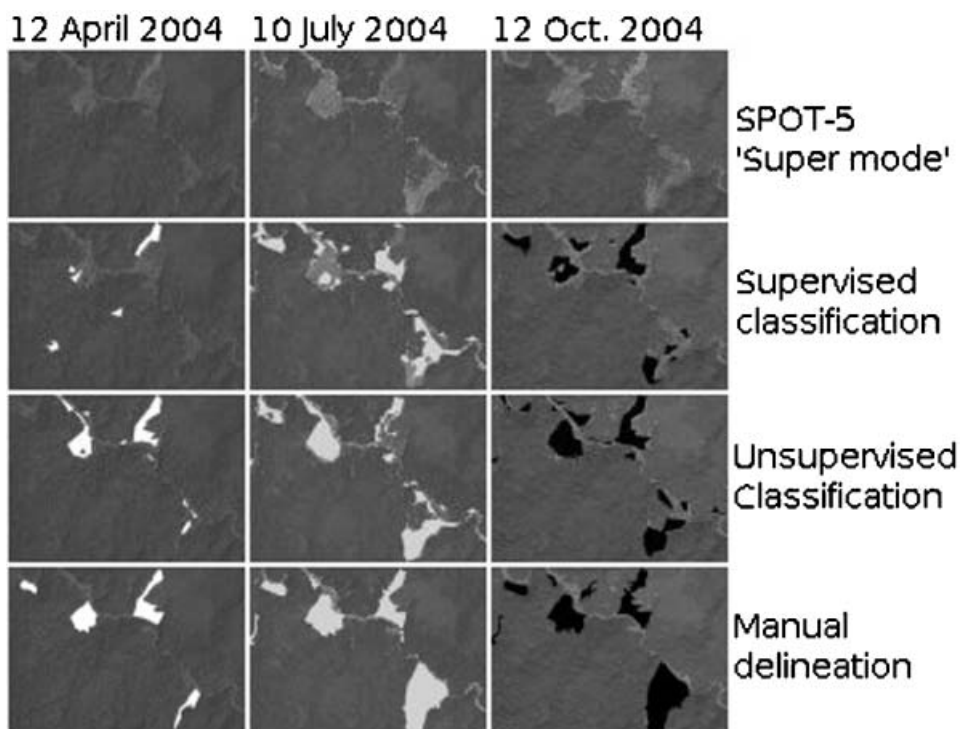
Figure 5.   SPOT-5 supermode imagery and classification results from the automated and manual methods for a select area for three different acquisition dates.

18.70 ha to 24.89 ha. The overlap of large landslide areas with the manual method probably accounts for the higher area concordance for the unsupervised classification.

   The validation by 0.35 m resolution orthophotographs confirmed the errors of omission and commission that were made by all three methods. Counter intuitively, we found that the automated method using 10 m resolution multi-spectral images was able to correctly identify many small landslides around 10 m wide that could not be positively identified in the 2.5 m supermode imagery.

   The application of a 28° slope mask to filter out non-vegetated features with relatively low slopes that were not landslides was not fully successful. This can be explained as follows. The slope mask had a resolution of 40 m; therefore, 10 m to 15 m wide roads, parts of riverbeds and parts of farm fields close to steep hill slopes would still remain in the scene and be wrongly classified as landslides.

7.   Conclusion

In this study we tested automated classification methods and manual delineation of SPOT-5 products for mapping typhoon-triggered landslides. Unsupervised classi-fication using all SPOT-5 wavelength bands combined with a slope mask produced a 63% area concordance with manual mapping results using 2.5 m supermode imagery. Statistical tests revealed that the automated methods tended to produce significantly smaller landslide areas when compared to the manual delineation

results. Classification results were validated by 0.35 m orthophotographs and showed many errors of omission by the manual delineation method for small landslides. In contrast, the majority of errors made by the automated methods were errors of commission that could be attributed to the presence of roads, riverbeds and bare farm fields in the scene. When a higher resolution DEM becomes available, we believe that these errors can be reduced to a minimum, thus enabling a cost and time effective classification of landslides based on medium- and high-resolution multi-spectral satellite imagery.

Acknowledgments

References

ALEOTTI, P. and CHOWDHURY, R., 1999, Landslide hazard assessment: summary review and new perspectives. *Bulletin of Engineering Geology and the Environment*, **58**, pp. 21–44.

BORGHUIS, A.M. and CHIU, Y.J., 2005, Reconstructing more than 40 years of soil redistribution in two Taiwanese mountainous watersheds. *Proceedings of the 2005 European Regional Science Association (ERSA) Conference*, Vrije Universiteit, Amsterdam, The Netherlands.

CHADWICK, J., DORSCH, S., GLENN, N., THACKRAY, G. and SHILLING, K., 2005, Application of multi-temporal high-resolution imagery and GPS in a study of the motion of a canyon rim landslide. *ISPRS Journal of Photogrammetry & Remote Sensing*, **59**, pp. 212–221.

CHANG, K., 2006, *Introduction to Geographic Information Systems*, 3rd edn (New York: McGraw-Hill).

CHANG, J.C. and SLAYMAKER, O., 2002, Frequency and spatial distribution of landslides in a mountainous drainage basin: Western Foothills, Taiwan. *Catena*, **46**, pp. 285–307.

CRUDEN, D.M., 1991, A simple definition of a landslide. *Bulletin of the International Association of Engineering Geology*, **43**, pp. 27–29.

CWB (CENTRAL WEATHER BUREAU), 2004a, http://photino.cwb.gov.tw/tyweb/tyfnweb/htm/2004mindulle.htm (accessed 22 April 2006).

CWB (CENTRAL WEATHER BUREAU), 2004b, http://photino.cwb.gov.tw/tyweb/tyfnweb/htm/2004aere.htm (accessed 22 April 2006).

DADSON, S.J., HOVIUS, N., CHEN, H., DADE, B.W., LIN, J.C., HSU, M.L., LIN, C.W., HORNG, M.J., CHEN, T.C., MILLIMAN, J. and STARK, C.P., 2004, Earthquake-triggered increase in sediment delivery from an active mountain belt. *Geology*, **32**, pp. 733–736.

DIKAU, R., 1999, The recognition of landslides. In R. Casale and C. Margottini (Eds). *Floods and Landslides: Integrated Risk Assessment*, pp. 39–44 (Berlin: Springer).

HAEBERLIN, Y., TURBERG, P., RETIÈRE SENEGAS, O. and PARRIAUX, A., 2004, Validation of SPOT-5 satellite imagery for geological hazard identification and risk assessment for landslides, mud and debris flows in Matagalpa, Nicaragua. *Proceedings of the XXth ISPRS Congress*, Istanbul, Turkey, http://www.isprs.org/istanbul2004/comm1/papers/51.pdf (accessed 22 April 2006).

HWANG, J.S., 1994, A study of the sustainable water resources system in Taiwan considering the problems of reservoir desilting. Taiwan Provincial Water Conservancy Bureau, Taichung City, Taiwan.

KORUP, O., 2004, Geomorphometric characteristics of New Zealand landslide dams. *Engineering Geology*, **73**, pp. 13–35.

LILLESAND, T.M., KIEFER, R.W. and CHIPMAN, J.W., 2004, *Remote Sensing and Image Interpretation*, 5th edn (New York: Wiley).

LIU, J., WONG, C., HUANG, J. and YANG, M., 2002, Landslide-enhancement images for the study of torrential-rainfall landslides. *Proceedings of the 23rd Asian Conference on Remote Sensing (ACRS 2002)*, Kathmandu, Nepal, http://www.gisdevelopment.net/ aars/acrs/2002/env/193.pdf (accessed 22 April 2006).

LIU, J. and WOING, T., 1999, A practical approach to creating a landslide database using Taiwan SPOT mosaic. *Proceedings of the 20th Asian Conference on Remote Sensing (ACRS 1999)*, Hong Kong, China, http://www.gisdevelopment.net/aars/acrs/1999/ ts12/ts12513.asp (accessed 22 April 2006).

NETELER, M. and MITASOVA, H., 2004, Thematic reclassification of satellite data. In *Open Source GIS: A GRASS GIS Approach*, 2nd edn, Chapter 9.8 (Berlin: Springer).

NICHOLS, J. and WONG, M.S., 2004, Satellite remote sensing for detailed landslide inventories using change detection and image fusion. *International Journal of Remote Sensing*, **29**, pp. 1913–1926.

PETLEY, D.N., CRICK, W.D.O. and HART, A.B., 2002, The use of satellite imagery in landslide studies in high mountain area. *Proceedings of the 23rd Asian Conference on Remote Sensing (ACRS 2002)*, Kathmandu, Nepal, http://www.gisdevelopment.net/aars/acrs/ 2002/hdm/48.pdf (accessed 22 April 2006).

RAMLI, M.F. and PETLEY, D.N., 2006, Best band combination for landslide studies in temperate environments. *International Journal of Remote Sensing*, **27**, pp. 1219–1231.

ROSIN, P.L. and HERVÁS, J., 2005, Remote sensing image thresholding methods for determining landslide activity. *International Journal of Remote Sensing*, **26**, pp. 1075–1092.

SWCB (SOIL AND WATER CONSERVATION BUREAU), 2003, Soil and Water Conservation Law. Taipei City, Taiwan. (in Chinese).

VOHORA, V.K. and DONOGHUE, S.L., 2004, Application of remote sensing data to landslide mapping in Hong Kong. *Proceedings of the XXth ISPRS Congress*, Istanbul, Turkey, http://www.isprs.org/istanbul2004/comm4/papers/398.pdf (accessed 22 April 2006).